PCCP

First Principles Density Functional Theory Study of Tritium Species Adsorption on Ni(111) Surface and Diffusion in Nickel-sublayer for Tritium Storage

Journal:	*Physical Chemistry Chemical Physics*
Manuscript ID	CP-ART-11-2024-004398.R1
Article Type:	Paper
Date Submitted by the Author:	27-Nov-2024
Complete List of Authors:	Tafen, De Nyago; National Energy Technology Laboratory Paudel, Hari; National Energy Technology Laboratory, Functional Materials Engineering Casella, Andrew; Pacific Northwest National Laboratory Senor, David; PNNL Duan, Yuhua; National Energy Technology Laboratory

ARTICLE

First Principles Density Functional Theory Study of Tritium Species Adsorption on Ni(111) Surface and Diffusion in Nickel-Sublayer for Tritium Storage

Received 00th January 20xx,
Accepted 00th January 20xx

DOI: 10.1039/x0xx00000x

De Nyago Tafen[a,b], Hari P. Paudel[c,d], David J. Senor[e], Andrew M. Casella[e], and Yuhua Duan[c,*]

The nickel-plated zircaloy-4 is used as a tritium (^3H) getter in the tritium-producing burnable absorber rods (TPBARs) to capture ^3H produced in the ^6Li-riched annular γ-$LiAlO_2$ pellet under neutron irradiation. The experimental data and our previous theoretical results showed that the ^3H species produced from the γ-$LiAlO_2$ pellet were mainly $^3H_2$ and ^3H_2O. These ^3H species diffuse from the surface of the $LiAlO_2$ pellet across vacuum to the nickel-plated zircaloy-4 getter and then further diffuse into the getter to chemically form metal hydrides. While a number of studies show that oxygen binds strongly as compared to ^3H on the nickel (Ni) layer, the detailed mechanism of ^3H species absorption and diffusion across the Ni plate and Ni/Zr interface are still unclear. By employing density functional theory calculations, here we explored the $^3H_2$ and ^3H_2O species adsorption and dissociation on the Ni (111) surface and diffusion into the Ni sublayer. Our results indicated that the $^3H_2$ and ^3H_2O dissociate on the Ni (111) surface. The NiO_x and $Ni(O^3H)_x$ could be formed in the Ni layer due to the higher oxygen (O) diffusion energy barrier and formation of Ni vacancy defects. The oxygen was found to be retained in the Ni layer from diffusing across the Ni-Zr interface. This was revealed by comparing the diffusion barriers for ^3H with O. ^3H was found to have nearly three times smaller diffusion barrier than for O, making ^3H comparatively easier to diffuse through the Ni layer. The obtained results provide guidelines for experimental measurements on ^3H retention behavior in TPBARs and may open further avenues to explore the impurity effects on ^3H diffusion and storage at the Ni/Zircaloy interfaces.

Introduction

Zirconium (Zr) and its alloys (Zircaloy-4) are widely used in nuclear reactors due to their low neutron absorption cross-section and excellent corrosion resistance.[1-3] In tritium-producing burnable absorber rods (TPBARs), the metal getter tube located between the cladding and the γ-$LiAlO_2$ pellets is composed of nickel (Ni)-plated Zircaloy-4, which is used to capture tritium (^3H) species (mainly $^3H_2$ and ^3H_2O) generated from γ-$LiAlO_2$ pellets during irradiation.[4] The ^3H-related products transfer to the surface of metal Ni upon adsorption and dissociation to form new ^3H species and diffuse into the Zircaloy-4 getters to form metal hydrides (Zr^3H_x). Therefore, exploring ^3H species ($^3H_2$, ^3H_2O) dissociation on the surface of Ni and diffusion across the interface of Ni-plated Zircaloy-4 getters can provide a better understanding of ^3H species formation and transport from pellets into the getters.

In recent years, we conducted a series of studies on γ-$LiAlO_2$ pellets to understand the tritium products and their transport through the pellet materials. [2, 5-7] Aside from studying the surface properties of γ-$LiAlO_2$, we also explored the diffusion of ^3H and O^3H species on its defective (100) and (101) surfaces, and the ^3H_2O formation and desorption from the γ-$LiAlO_2$ (101) and $LiAl_5O_8$ (111) surfaces. [8-13] In our earlier studies, we found that the $^3H_2$ molecule is the main product initially released from the pellets. With increasing the number of Li vacancies and ^3H atoms under irradiation, ^3H_2O can be formed and released from the pellets as well. Although we explored ^3H diffusion in different zirconium hydrides, [3, 14, 15], there remained open questions that needed answers: (i) how and which ^3H species (^3H, O^3H, O, or $^3H_2$, etc.) do diffuse into Zircaloy-4 from the surface of γ-$LiAlO_2$ pellets? (ii) In the case of ^3H_2O, can the Ni coating layer retain O by forming NiO_x or $Ni(O^3H)_x$ to prevent O diffusion into Zircalory-4 getter? Detail answers to these questions provide understanding of NiO_x or $Ni(O^3H)_x$ phase formation at various concentration of O and its impact on the ^3H and O adsorption and diffusion in Ni layer.

In TPBARs, the $^3H_2$ and ^3H_2O molecules generated from the γ-$LiAlO_2$ pellets[8-13] are transported to the Ni-plated Zircaloy-4 getters. The adsorption and diffusion processes in Ni layer directly impacts the ^3H retention rate at the getter. To capture the chemical adsorption kinetics in Ni layer and diffusion process across the Ni and Zrcaloy-4 interface, it is essential to include accurate electronic and magnetic properties of Ni. While the classical diffusion model where diffusion coefficient is extracted from the Brownian motion combined with adsorption/desorption and particle displacement distributions at single molecular levels could provide insight migration and displacement mechanisms for large interfaces, and fluid

[a] National Energy Technology Laboratory, 1450 Queen Avenue SW, Albany, OR 97321 USA.
[b] NETL Support Contractor, 1450 Queen Avenue SW, Albany, OR 97321 USA.
[c] National Energy Technology Laboratory, 626 Cochran Mill Road, Pittsburgh, PA 15236, USA
[d] NETL Support Contractor, 626 Cochran Mill Road, Pittsburgh, PA 15236, USA.
[e] Pacific Northwest National Laboratory, 902 Battelle Boulevard, Richland, WA, 99354, USA
* To whom correspondence should be addressed. E-mail: Yuhua.duan@netl.doe.gov; Tel. 1-412-386-5771, Fax: 1-412-386-5990.

systems,[16] better understanding of diffusion mechanisms in solid systems with accurate electronic structures could be achieved using DFT level of calculations. The ^3H_2O molecules dissociate on Ni(111) surface according to the reaction mechanism: $^3H_2O \rightarrow O^3H + {}^3H$ and $O^3H + {}^3H \rightarrow O + {}^3H + {}^3H$. Previous studies showed that the first dissociation requires an activation energy of 0.68 eV, where ^3H_2O is dissociated into an O^3H and ^3H species.[26] The second process involves the dissociation of O^3H into O and ^3H and requires a higher activation barrier of 1.25 eV.[26] The ^3H_2O species are adsorbed on Ni(111) by occupying a top of a Ni atom, whereas the other three species, O^3H, ^3H, and O occupy a three-fold hollow site face centred cubic (fcc). As $^3H_2$ reaches the Ni(111) surface it dissociates into two atomic ^3H ($^3H_2 \rightarrow {}^3H + {}^3H$) with a low activation energy. Shirazi et al. obtained activation energies of 0.03 and 0.09 eV for H-coverage of 0.125 and 0.25 monolayer (ML), respectively.[27]

To fully address aforementioned open questions, in this study, we explored the $^3H_2$ and ^3H_2O molecules' dissociation on the surfaces of Ni-plated Zircaloy-4 getters to clarify the ^3H species that dissolve into the metal getters and calculated the diffusion pathways of these ^3H species in the bulk Ni phase to identify species that diffuse across the interface of Ni-plated Zircalory-4. While there are comprehensive studies of H_2 and H_2O adsorption on the surfaces of Ni available in the literature, [17, 18] here we targeted on the possibility of the nickel oxide/hydroxide (NiO_x, $Ni(O^3H)_x$) phase formation in the Ni-coated layer to prevent O diffusion into the Zircaloy-4 getter. We calculated the diffusion pathways of ^3H across such oxide/hydroxide layer into the Zircaloy-4 getter. By taking Ni (111) surface, we provided detail mechanisms for adsorption and diffusion pathways for ^3H. Our hypothesis here is that ^3H has a lower diffusion barrier in Ni than O, leading to higher chance of ^3H diffusion into the zircalloy getter. Particularly, we determined if O from ^3H_2O could be retained in the Ni layer to form the $NiO_x/Ni(O^3H)_x$ phase and let only ^3H diffuse to the Zircaloy-4 getter to form metal hydrides.

This paper is organized as follows. We first present theoretical and computational methodologies implemented in this work. . Then we present and discuss the results of our study on NiO species formation and the diffusion mechanisms for 3H in Ni surfaces and subsurface. Finally, we summarize our work and provide further outlook.

Theoretical and Computational Methods

All the calculations were performed based on density functional theory (DFT) with the plane-wave basis set and the pseudopotential as implemented in the Vienna ab initio simulation package (VASP).[19-21] The electron-ion interaction is described with the projector augmented wave method (PAW).[22, 23] The exchange and correction energies are described within generalized gradient approximation using the spin-polarized Perdew-Burke-Ernzerhof formulation (GGA-PBE).[24] A cutoff energy of 400 eV was used for the plane wave expansion. The convergence criteria for geometry optimizations of total energy and force were 10^{-5} eV and 0.01 eV/Å, respectively. The pseudo-potential of ^3H was obtained by modifying the mass in the standard hydrogen (^1H) pseudo-potential. The surface slab was generated from the fully relaxed bulk structure. For the Ni (111) surfaces this study used a five-layered 4 × 4 supercell slab with a vacuum region of 12 Å along the z-axis to avoid interactions between periodically repeated slabs. The bottom two layers were kept fixed in their bulk positions as the rest of the slab including adsorbates were relaxed. The k-point sampling in a reciprocal space was generated using Monkhorst-Pack method and a 3 × 3 × 1 grid size.

Diffusion barriers for reactions were calculated using the climbing nudged elastic band (c-NEB) method.[25] For each simulation a minimum of five images were used. The energy difference between the two optimized minima gave the reaction energy. The diffusion barrier was defined as the difference between the transition state and the initial state energies.

Results and Discussion

Stability and Formation of NiO_x and/or $Ni(O^3H)_x$ Phase

Based on literature report, [26,27] we determined the mechanisms of dissociation of $^3H_2$ and ^3H_2O molecules on the Ni surfaces to clarify the ^3H species that dissolved into the metal getters. With such information, then we focused on the diffusion of these ^3H species in the Ni bulk and explored a possibility of forming NiO_x and/or $Ni(O^3H)_x$ phases. The stability of Ni metal and its derived compounds, including oxides, hydroxides, and oxyhydroxides can be predicted from DFT combined with thermodynamic analysis. To predict the stability and formation of the NiO_x and/or $Ni(O^3H)_x$ phase, we explored the most stable compounds of Ni oxides, hydroxides and oxyhydroxides observed experimentally (Table 1). We computed the equilibrium crystal structures, electronic structures, and thermodynamic energies using DFT with different options of exchange correlation potentials. In addition to the PBE functional, we used the hybrid functional HSE06 [28] and a PBE+U functional. The HSE06 tends to perform better especially when dealing with oxides. Electronic structures and thermodynamic analysis are combined together to determine the chemical potential domains of $Ni(O^3H)_x$ stability and phase formation.

(1) Calculations of Total and Formation Energies

The formation energy of a $Ni_xO_yH_z$ compound can be defined as follows:

$$\Delta H(Ni_xO_yH_z) = E_{DFT}(Ni_xO_yH_z) - x\mu_{Ni}^{solid} - y\mu_O^{gas} - z\mu_H^{gas} \quad (1)$$

where $E_{DFT}(Ni_xO_yH_z)$ is the DFT calculated total energy of the compound; μ_{Ni}^{solid}, μ_O^{gas}, and μ_H^{gas} are the chemical potentials of Ni, O, and H in their stable elemental solid/gas state; x, y, and z are coefficients of proportionality. Table 1 lists the DFT calculated total and formation energies of the most stable compounds of nickel oxides and hydroxides using different exchange correlation functionals. The formation energy ΔH for the PBE corrected and PBE+U corrected used a corrected value for the O_2 molecule. Our results for the formation energies are in good agreement with literature data.[29, 30] The computed total energies and formation energies of these compounds are used to determine the chemical potential domains for the formation of $Ni(O^3H)_x$.

ARTICLE

Table 1. Space groups, calculated total and formation energies (eV/f.u.) of Ni-O-H based compounds. Isotopes for H are specifically written as ^1H and ^3H.

Compound	Space group	Formula unit	Total energy HSE06	Total energy PBE	Total energy PBE+U	ΔH HSE06	ΔH PBE	ΔH PBE corrected	ΔH PBE+U corrected
Ni	Fm-3m	1	-6.448	-5.459	-1.842				
$^1H_2$		1	-7.713	-6.772	-6.772				
O_2		1	-17.036	-9.862	-9.862				
NiO	Fm-3m	2	-17.970	-11.655	-10.278	-3.004	-1.265	-1.945	-4.184
NiO_2	P-3m1	1	-25.491	-17.350	-14.277	-2.007	-2.029	-3.389	-3.933
Ni_2O_3	R-3c	2	-42.851	-29.648	-24.132	-4.402	-3.937	-5.977	-7.694
Ni_3O_4	Fd-3m	8	-61.366	-41.783	-34.696	-7.950	-5.681	-8.401	-12.165
$Ni(O^3H)_2$	P-3m1	1	-37.451	-26.220	-25.071	-6.255	-4.127	-5.487	-7.955
$NiOO^1H$	R-3m	2	-31.462	-22.124	-19.789	-4.122	-3.417	-4.777	-6.059

(2) Chemical Potential Domains for the Stability and Formation of $Ni(O^3H)_x$

The formation and stability of a system depend on the chemical potential of its constituent elements, which varies with specific equilibrium conditions. In the thermodynamic limits, the chemical potential domains for $Ni(O^3H)_2$ can be determined. The stability of $Ni(O^3H)_2$ against decomposition into its elemental constituents requires a smaller atomic chemical potential than the corresponding elemental solid, i.e.,

$$\mu_i \leq \mu_i^{solid/gas}, \quad i = Ni, H, O. \qquad (2)$$

Setting $\Delta\mu_i = \mu_i - \mu_i^{solid/gas}$, the above condition becomes

$$\Delta\mu_i \leq 0, \qquad i = Ni, H, O. \qquad (3)$$

For $\Delta\mu_i = 0$ we obtain a maximum i-rich condition. Thermodynamic equilibrium of a system requires that a sum of the chemical potentials of its constituent atoms be equal to its formation energy. Therefore, we can write:

$$\Delta\mu_{Ni} + 2\Delta\mu_O + 2\Delta\mu_H = \Delta H(Ni(OH)_2) \qquad (4)$$

where $\Delta H(Ni(OH)_2)$ is the formation energy of bulk $Ni(O^3H)_2$. To avoid the formation of other oxide compounds (such as NiO, NiO_2, Ni_2O_3, Ni_3O_4, NiOOH), the ranges of chemical potentials for the stability of $Ni(O^3H)_x$ are subject to the following additional criteria:

$$\Delta\mu_{Ni} + \Delta\mu_O \leq \Delta H(NiO) \qquad (5)$$

$$\Delta\mu_{Ni} + 2\Delta\mu_O \leq \Delta H(NiO_2) \qquad (6)$$

$$2\Delta\mu_{Ni} + 3\Delta\mu_O \leq \Delta H(Ni_2O_3) \qquad (7)$$

$$3\Delta\mu_{Ni} + 4\Delta\mu_O \leq \Delta H(Ni_3O_4) \qquad (8)$$

$$\Delta\mu_{Ni} + 2\Delta\mu_O + \Delta\mu_H \leq \Delta H(NiOOH) \qquad (9)$$

Combining Eq. 4 and Eqs. 5-9, we computed the chemical potential domains for the formation and stability of $Ni(O^3H)_2$ using the total energies and formation energies calculated above. Figure 1 shows the stable chemical potential region of the bulk $Ni(O^3H)_2$ in terms of the chemical potentials $\Delta\mu_O$,$\Delta\mu_{Ni}$, and $\Delta\mu_H$ using PBE and HSE06 functionals. The shaded area is the allowed chemical potential range for $Ni(O^3H)_2$ to be a stable phase. In the PBE functional, the limiting stable conditions are defined by five points with coordinates ($\Delta\mu_{Ni}$, $\Delta\mu_O$, $\Delta\mu_H$) namely A(-4.13, 0, 0), B(-2.71, 0, -0.71), C(-0.27, -1.22, -0.71), D(0, -1.42, -0.64), and E(0, -2.06, 0) with boundary lines formed by $Ni(O^3H)_2$, $NiOO^3H$, and Ni_3O_4. In contrast, the limiting stable conditions using the HSE06 functional is defined by the following four points with coordinates ($\Delta\mu_{Ni}$, $\Delta\mu_O$, $\Delta\mu_H$): A(-6.26, 0, 0), B(-3.00, 0, -1.63), C(0, -3.00, -0.12), and D(0, -3.13, 0) with boundary lines corresponding to $Ni(O^3H)_2$ and NiO.

To understand the discrepancy between the results from the PBE and HSE06 functionals, we look at the formation energy per atom for nickel oxide compounds. In Figure 2, we compare the formation energy per atom of the oxide compounds obtained using PBE, HSE06, and PBE+U functionals. The results show that HSE06 correctly predicts NiO as the most stable among all Ni oxides in agreement with the experiments, whereas PBE incorrectly assigns the lowest formation energy to Ni_3O_4.[31] PBE+U follows the same trend as HSE06. Our results also show that the formation energy per atom of $Ni(O^3H)_2$ is lower than that of $NiOO^3H$ in HSE06 (-1.25 eV/at vs. -1.03 eV/at), but it is the reverse in PBE (-0.82 eV/at vs. -0.85 eV/at). Our results agree with that of Huang *et al*. who studied the role of the exchange interactions on the accuracy of the electrochemical phase diagrams of Ni using first-principles methods.[29] They observed that the simulation accuracy tends to increase going from semi-local functionals to non-local hybrid functionals due to the increased electronic exchange attraction. Overall, we found that the HSE06 and PBE + U functionals correctly predict

NiO as the most stable oxide. The chemical potential domains are better described using the HSE06 functional.

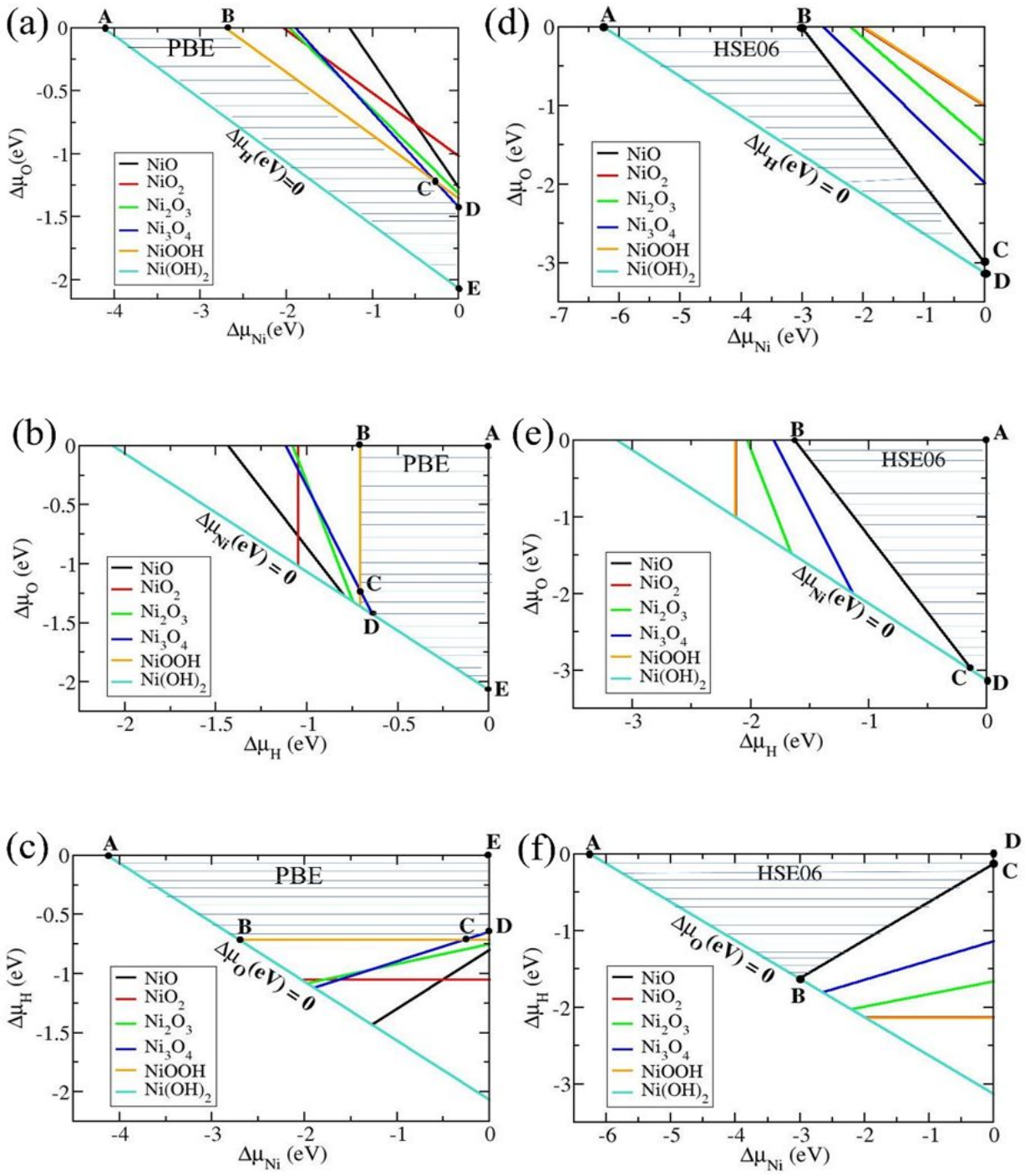

Figure 1. The allowed chemical potential domains (shaded regions determined by A, B, C, D, and E) for $Ni(O^3H)_2$ to be stable. (a), (b) and (c) are results obtained using the PBE functional. (d), (e), and (f) are results obtained using the HSE06 functional. The secondary phases which are indicated by color-coded lines restrict the stable phase.

Determining the ^{3}H Species Dissolve from Surface into Ni Bulk

(1) Tritium (^{3}H) Diffusion from Ni(111) Surface to Bulk

We first calculated the diffusion of a single ^{3}H atom into a pure Ni(111) surface. ^{3}H species diffused on the surface and occupied an interstitial site in the subsurface. There are two possible interstitial sites in the bulk Ni: a tetrahedral (denoted tetra) site

and an octahedral (denoted octah) site. Figure 3 shows the migration of ^3H species from the surface into bulk. The calculated migration barrier of ^3H from a fcc surface to a subsurface octahedral site is 0.698 eV. The reaction is endothermic by 0.621 eV with activation energy for resurfacing 0.077 eV. This result is in good agreement with previous calculations.[27, 32-34] Shirazi et al. found an activation energy of 0.64 eV for a H-coverage of 0.50 monolayer and a resurfacing energy barrier of 0.05 eV.[27] Henkelman et al. calculated energy barriers of 0.6 eV and 0.1 eV for the diffusion of H to the subsurface and the resurfacing of H, respectively.[32] An octahedral subsurface H can diffuse into the bulk via a tetrahedral site with an activation energy of 0.454 eV. Greeley and Mavrikakis found an energy barrier of 0.52 eV.[35]

(2) Migration of ^3H Species from Surface to Subsurface after ^3H_2O Dissociation

Next, we investigated the diffusion of ^3H into the surface after a ^3H_2O dissociation at partial and complete dissociation. In the partial dissociation, we have an ^3H and O^3H species lying on the surface. In complete dissociation, we have two ^3H species and an O species lying on the surface. Our results in Figure 4 show a slightly lower diffusion barrier for ^3H in the case of a complete dissociation (0.572 eV) compared to that in the partial dissociation (0.618 eV). These two barriers are lower than that of a single ^3H atom on the surface diffusing into the subsurface. As ^3H_2O dissociates, surface sites are occupied which increases surface coverage leading to a redistribution of electron density. The increase of surface coverage is accompanied by a reduction in activation energy of the diffusion of a surface-bound ^3H-atom to the subsurface.

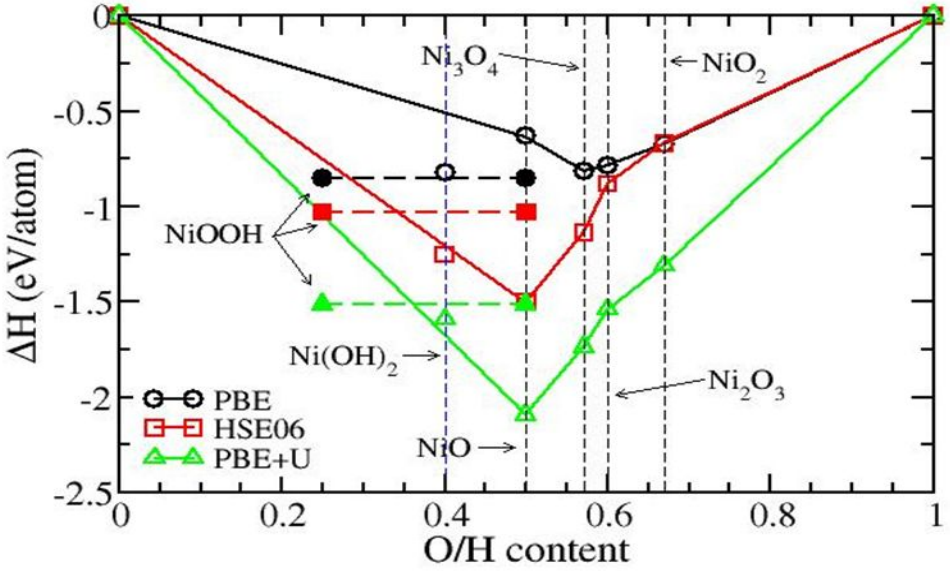

Figure 2. Formation energies per atom from PBE, HSE06, and PBE+U functionals for nickel oxide compounds. The blue dashed line connects the formation energies of $Ni(O^3H)_2$ with equal O and ^3H content, 0.4. Horizontal dashed lines with solid symbols connect the formation energies of $NiOO^3H$ with O content 0.5 and ^3H content 0.25.

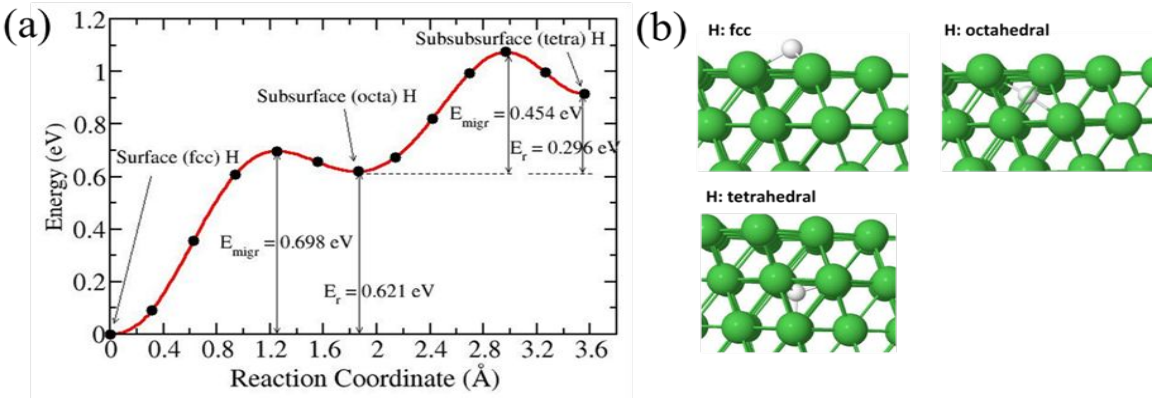

Figure 3. Energy barrier and transition pathway for H diffusing into a pure Ni(111) surface.

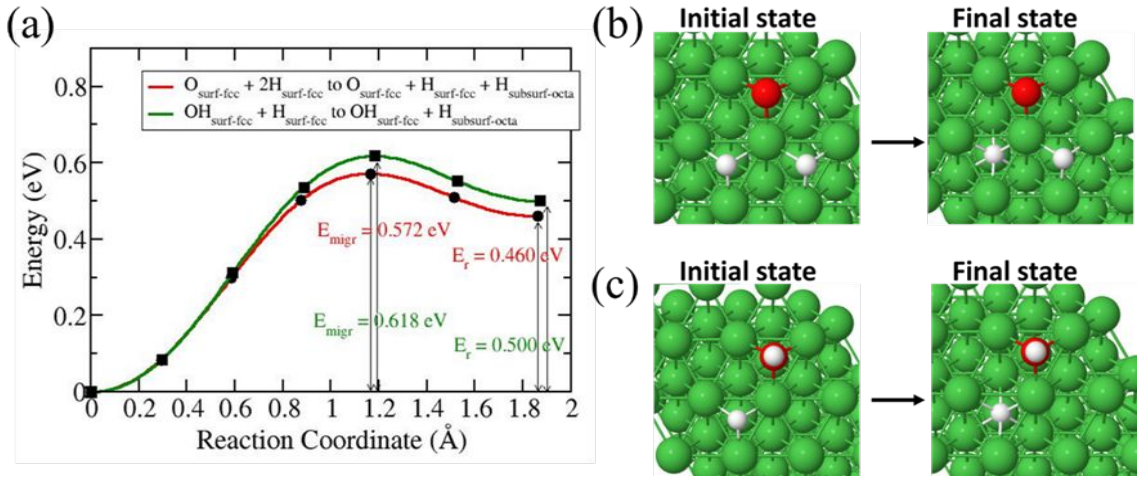

Figure 4. Energy barrier of ^3H species migration from surface to subsurface after ^3H_2O dissociation. Structures of the initial and final states.

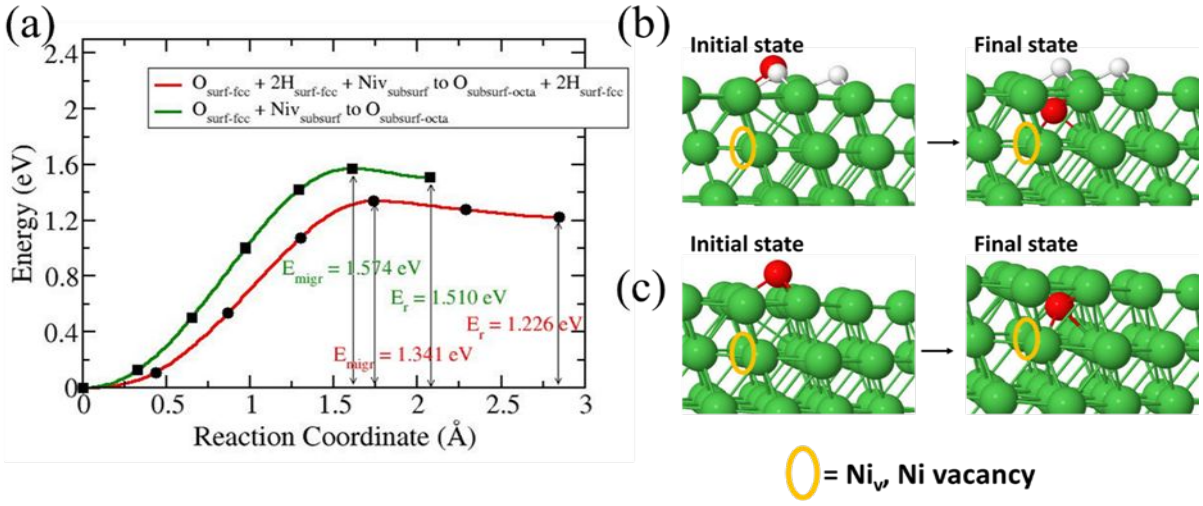

Figure 5. Migration barrier of O species diffusion into Ni(111) surface. Structures of the initial and final states (b) after ^3H_2O dissociation and (c) in bare surface. Orange circle denotes the location of Ni vacancy.

(3) Migration of O Species from Surface to Subsurface

The migration of O species from a fcc surface site to a subsurface octahedral requires the presence of a defect such as Ni vacancy.[36] Our study reveals that in the absence of Ni vacancy O diffusion into the surface is unfavourable. We studied the diffusion of O species in a pure Ni surface with a subsurface V_{Ni} and the diffusion of O after an ^3H_2O dissociation (Figure 5). Our calculations reveal that presence of ^3H helps to reduce the diffusion barrier for O in the Ni(111) surface than in presence of a subsurface V_{Ni} and without ^3H. In the presence of ^3H the activation energy and reaction energy are 1.341 eV and 1.226 eV, respectively, as compared to 1.574 eV and 1.510 eV for pure Ni surface with a subsurface V_{Ni}.

The diffusion barrier for ^3H is lower than that for O on the Ni surface and bulk. Therefore, it is favourable for ^3H to pass through the Ni coating and reach the Ni-Zircalory-4 interface. The calculated diffusion barrier for O is nearly three times that for the diffusion of ^3H. Experimentally, Ebisuzki et al.[37] and Lu et al.[38] obtained the diffusion barriers for H in Ni to be 0.42 and 0.19 eV, respectively. Lu et al.[38] also predicted the trapping of H in Ni using electrochemical permeation test and thermal desorption spectroscopy (TDS) and found the reversible trapping energy to be 0.26 eV. Similarly, Zholobov et al[39] and Park et al[40] experimentally predicted the diffusion barrier for O in Ni to be 1.89 and 1.70 eV, respectively.. These results together with our calculated values indicate that ^3H has much higher probability to diffuse through the Ni surface as compared to O.

ARTICLE

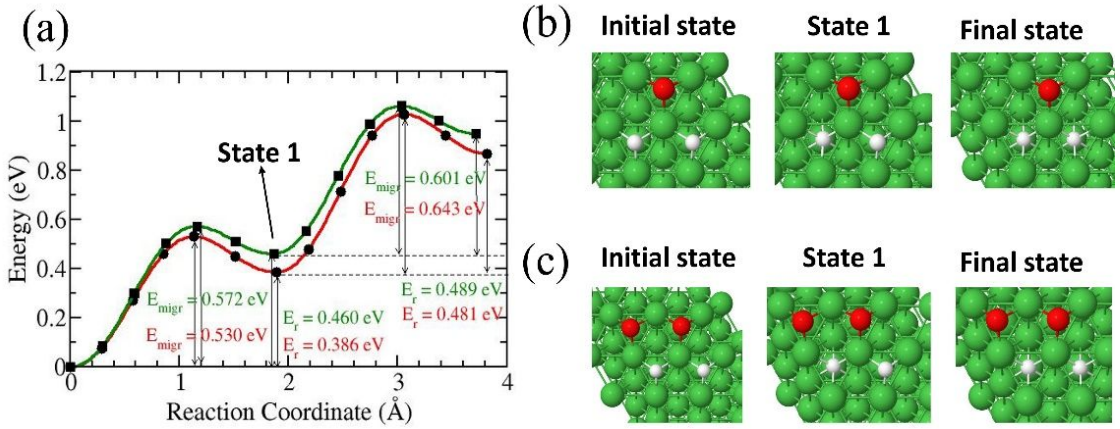

Figure 6. (a) Migration barrier and reaction energies of two ^3H species on Ni surface after ^3H_2O dissociation [41], and in the presence of two surface O species (green) Structures of the initial and final states (b) for the two ^3H species on Ni surface after ^3H_2O dissociation and (c) in the presence of two surface O species.

(4) Diffusion of Two ^3H Species into Nickel Surface in the Presence of O Surface Species

In this section, we studied the diffusion of two ^3H species into Ni(111) surface in the presence of surface O and O^3H species. Three different cases were investigated.

(a) One O Surface Species

We studied the diffusion of two ^3H atoms into Ni(111) surface after a ^3H_2O dissociation. The first ^3H is found to migrate into the subsurface with an energy barrier of 0.572 eV while the second ^3H is found to have an energy barrier of 0.601 eV (Figure 6). The presence of a second ^3H on the surface contributes to the lowering of the migration barrier for the first ^3H.

(b) Two O Surface Species

We also studied the diffusion of two ^3H species in the presence of two O surface species (Figure 6). The first ^3H migrates into the surface with an even lower barrier and a lower reaction energy compared to the previous cases. The second ^3H diffuses with a higher diffusion barrier of 0.643 eV and a reaction energy of 0.481 eV.

(c) O and O^3H Surface Species

To understand the effect of O and O^3H after disassociation of ^3H_2O, we calculated the diffusion of ^3H in the presence of O and O^3H surface species. The results show that ^3H diffuses with a migration barrier of 0.562 eV and a reaction energy of 0.403 eV (Figure 7). This barrier is much lower than the barrier of a single ^3H diffusing on a pure and undefective Ni(111) surface.

In all three cases, the diffusion of ^3H on the surface is favourable compared to that of O. We also investigated the diffusion of ^3H from the surface to the subsurface in the presence of an O at the octahedral site (Figure 7). Our results reveal that ^3H diffuses into a subsurface octahedral site with an energy barrier of 0.595 eV and endothermic reaction energy of 0.452 eV.

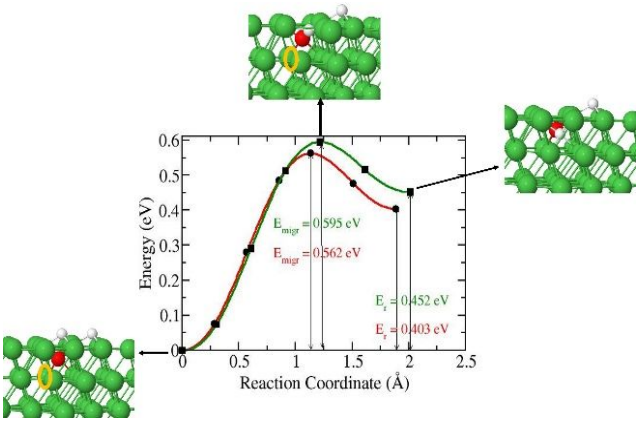

Figure7. Migration barrier and reaction energy of the diffusion of ^3H on the surface in presence of O and O^3H species [41] and in the presence of an O in a subsurface octahedral (green) The insets are the initial, transition and final states for the O in a subsurface octahedral.

Identifying the Energy Barrier of ^3H Species Diffusion in the Ni Bulk

In this section, we investigate the diffusion of ^3H in Ni bulk and the formation of $Ni(O^3H)_x$. We started with the assumption that an O migrates into the subsurface and we studied the diffusion

of a ^3H species toward O to form $Ni(O^3H)_x$. We studied three different cases with the third case consisting of diffusion of O^3H from the surface into the subsurface. However, O^3H diffusion into the surface is unfavourable.

(1) Case1: Formation of $Ni(O^3H)_x$ through Diffusion of a Subsurface H Species

In this case, a ^3H species in a subsurface octahedral site is allowed to diffuse toward O to form a $Ni(O^3H)_x$ unit. We obtained an activation barrier of ~ 0.55 eV for the diffusion of ^3H and formation of $Ni(O^3H)_x$. The reaction is endothermic by 0.125 eV as shown in Figure 8.

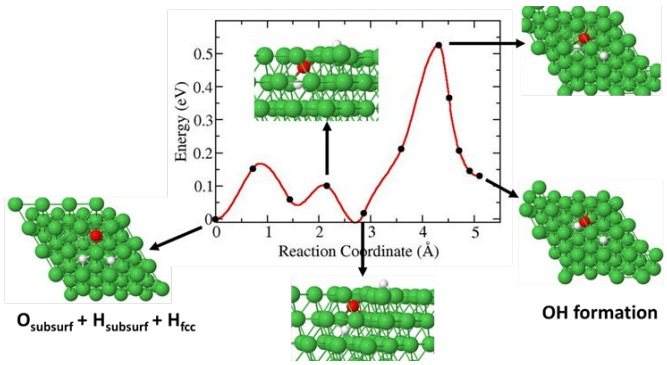

Figure 8. Diffusion barrier and diffusion pathways for subsurface ^3H diffusion and $Ni(O^3H)_x$ formation.

(2) Case 2: Formation of $Ni(O^3H)_x$ through Diffusion of a Surface ^3H Species

In this case, a surface ^3H species is allowed to diffuse in the surface through a hexagonal closest packed (hcp) site close to the subsurface O species. As shown in Figure 9, our calculated pathways show that ^3H on a fcc site migrate to a hcp surface site with an energy barrier of ~ 0.2 eV. Then it diffuses into a subsurface octahedral site away from the subsurface O with an activation energy of 0.87 eV. This barrier is 0.27 eV higher than that of a ^3H, migrating from a surface fcc site (Figure 7). Finally, the diffusing ^3H must overcome a barrier of ~ 1eV to form a $Ni(O^3H)_x$ complex.

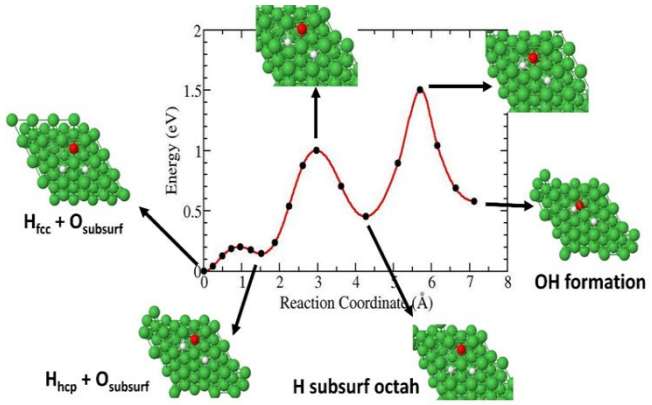

Figure 9. Diffusion barrier and transition pathways for ^3H diffusion into surface and subsurface formation of $Ni(O^3H)_x$.

This study also investigated the diffusion of O species from a subsurface octahedral to a sub-subsurface octahedral. The results show a diffusion barrier of less than 0.4 eV as shown in Figure 10.

David et al. calculated the migration energies of the diffusion along octah-tetrah for O atoms in Ni bulk and found 0.75 eV.[42] Previous work from Fang et al. revealed that for O to diffuse into nickel bulk requires an activation energy of at least 1.68 eV.[43]

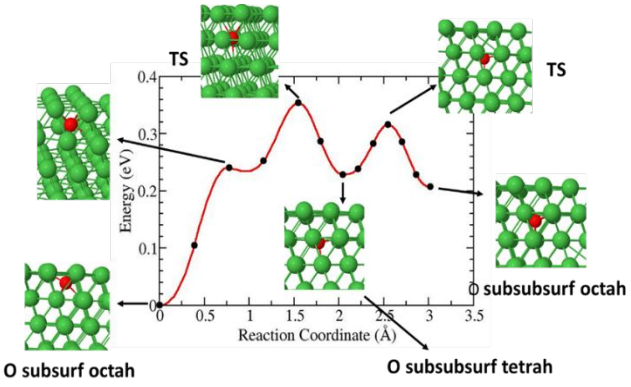

Figure 10. Diffusion barrier and reaction pathways of O species from a subsurface octahedral to a sub-subsurface octahedral.

Summary and Conclusions

Formation of chemical compounds O^3H, ^3H_2O, and metal oxide on the Ni surface and subsurface regions can significantly affect adsorption, desorption, diffusion, and hinder ^3H and $^3H_2$ reaching out to the getter material. Experimental evidence shows the presence of above compounds including hydrocarbons forming in Ni and getter materials. In this study, we explored $^3H_2$ and ^3H_2O binding sites and their dissociation on the pure and defective (111) surface of Ni. As it is evident from the earlier studies, the possible dissociation steps of ^3H_2O are $^3H_2O \rightarrow O^3H + {}^3H \rightarrow O + {}^3H + {}^3H$, and $^3H_2 \rightarrow {}^3H + {}^3H$. Our calculations also showed that there is a stable chemical potential region where NiO_x or $Ni(O^3H)_x$ phases could form. We found that the HSE06 and PBE + U functionals more accurately predict NiO as the most stable oxide as compared other methods employed in this study for the formation energy calculations. The $^3H_2$ and ^3H_2O dissociated on the surface of Ni could diffuse into the subsurface region. We found that the presence of ^3H on the surface reduces diffusion barriers for O by more than 15 %. The results for the calculation on diffusion barriers showed that O prefers to chemically bind in the Ni layer to form NiO_x or $Ni(O^3H)_x$. This was evident from the fact that it the calculated diffusion barrier for 3H is 0.48 eV, which is nearly three times smaller than the corresponding value for O in the Ni(111) surface. In addition, we also found that formation of NiO_x or $Ni(O^3H)_x$ phase in Ni subsurface layer is limited by diffusion of O and formation of Ni vacancies. We conclude that ^3H has higher probability of diffusion through the Ni layer and reaching out to the getter materials as compared to O.

Author contributions

Conceptualization, Y.D. and H.P.; methodology, D.T.; software, Y.D.; validation, D.T.; formal analysis, D.T.; investigation, D.T.; resources, Y.D., D.S., and A. C.; data curation, D.T.; writing—original draft preparation, D.T.; writing—review and editing, H.P., D.S., A.C. and Y.D.; visualization, D.T.; supervision, Y.D.; project administration, Y.D and A.C..; funding acquisition, D.S. and A.C. All authors have read and agreed to the published version of the manuscript.

Conflicts of interest

There are no conflicts to declare.

Data availability

The raw/processed data required to reproduce these findings cannot be shared at this time due to technical or time limitations but may be obtained by contacting corresponding author. The VASP software can be found at www.vasp.at. The version of VASP employed for this study is 5.4.4

Acknowledgements

This research was funded by the National Nuclear Security Administration (NNSA) of the U. S. Department of Energy (DOE) through the Tritium Science Research Supporting the Tritium Modernization Program managed by Pacific Northwest National Laboratory (PNNL). This project was also funded by the United States Department of Energy, National Energy Technology Laboratory, in part, through a site support contract. Neither the United States Government nor any agency thereof, nor any of their employees, nor the support contractor, nor any of their employees, makes any warranty, express or implied, or assumes any legal liability or responsibility for the accuracy, completeness, or usefulness of any information, apparatus, product, or process disclosed, or represents that its use would not infringe privately owned rights. Reference herein to any specific commercial product, process, or service by trade name, trademark, manufacturer, or otherwise does not necessarily constitute or imply its endorsement, recommendation, or favouring by the United States Government or any agency thereof. The views and opinions of authors expressed herein do not necessarily state or reflect those of the United States Government or any agency thereof.

Notes and references

1. J. J. Kearns, *J Nucl Mater*, 1972, **43**, 330-338.
2. H. Paudel, Y. L. Lee, D. Senor and Y. Duan, *J Phys Chem C*, 2018, **122**, 9755-9765
3. C. M. Andolina, W. A. Saidi, H. P. Paudel, D. J. Senor and Y. Duan, *Comp Mater Sci*, 2022, **209**, 111384.
4. D. J. Senor, *Recommendations for Science and Technology in Support of the Tritium Sustainment Program, PNNL-27216, Rev.1*, PNNL, 2018.
5. H. P. Paudel and Y. Duan, *J Phys Chem C*, 2018, **122**, 28447-28459.
6. Y.-L. Lee, J. Holber, H. P. Paudel, D. C. Sorescu, D. J. Senor and Y. Duan, *J Nucl Mater*, 2018, **511**, 375-389.
7. Y. Duan, D. C. Sorescu, W. L. Jiang and D. J. Senor, *J Nucl Mater*, 2020, **530**, 152963.
8. T. Jia, D. J. Senor and Y. Duan, *Comp Mater Sci*, 2020, **181**, 109748.
9. T. Jia, D. J. Senor and Y. Duan, *J Nucl Mater*, 2020, **540**, 152394.
10. T. Jia, D. J. Senor and Y. Duan, *Applied Surface Science Advances*, 2021, **5**, 100114.
11. T. Jia, D. J. Senor and Y. Duan, *J Nucl Mater*, 2021, **555**, 153111.
12. T. Jia, Z. Zeng, H. Paudel, D. J. Senor and Y. Duan, *J Nucl Mater*, 2019, **522**, 1-10.
13. H. P. Paudel, D. J. Senor and Y. Duan, *Comp Mater Sci*, 2021, **193**, 110419.
14. T. Jia, H. P. Paudel, D. J. Senor and Y. Duan, *Comp Mater Sci*, 2022, **203**, 111158.
15. H. P. Paudel, T. Jia, W. A. Saidi, D. J. Senor, A. M. Casella and Y. Duan, *The Journal of Physical Chemistry C*, 2023, **127**, 12435-12443.
16. A. Díez Fernández, P. Charchar, A. G. Cherstvy, R. Metzler and M. W. Finnis, *Physical Chemistry Chemical Physics*, 2020, **22**, 27955-27965.
17. J. Carrasco, A. Hodgson and A. Michaelides, *Nature Materials*, 2012, **11**, 667-674.
18. K. Christmann, R. J. Behm, G. Ertl, M. A. Van Hove and W. H. Weinberg, *The Journal of Chemical Physics*, 2008, **70**, 4168-4184.
19. G. Kresse and J. Furthmuller, *Comp Mater Sci*, 1996, **6**, 15-50.
20. G. Kresse and J. Furthmuller, *Phys. Rev. B*, 1996, **54**, 11169-11186.
21. G. Kresse and J. Hafner, *Phys Rev B*, 1993, **47**, 558-561.
22. P. E. Blöchl, *Phys Rev B*, 1994, **50**, 17953-17979.
23. G. Kresse and D. Joubert, *Phys Rev B*, 1999, **59**, 1758-1775.
24. J. P. Perdew, K. Burke and M. Ernzerhof, *Physical Review Letters*, 1996, **77**, 3865-3868.
25. G. Henkelman, B. P. Uberuaga and H. Jónsson, *The Journal of Chemical Physics*, 2000, **113**, 9901-9904.
26. L. Zhu, C. Liu, X. Wen, Y.-W. Li and H. Jiao, *Catalysis Science & Technology*, 2019, **9**, 199-212.
27. M. Shirazi, A. Bogaerts and E. C. Neyts, *Physical Chemistry Chemical Physics*, 2017, **19**, 19150-19158.
28. J. Heyd, G. E. Scuseria and M. Ernzerhof, *The Journal of Chemical Physics*, 2003, **118**, 8207-8215.
29. L.-F. Huang and J. M. Rondinelli, *Journal of Physics: Condensed Matter*, 2017, **29**, 475501.
30. A. Jain, S. P. Ong, G. Hautier, W. Chen, W. D. Richards, S. Dacek, S. Cholia, D. Gunter, D. Skinner, G. Ceder and K. A. Persson, *APL Materials*, 2013, **1**, 011002.
31. B. Beverskog and I. Puigdomenech, *Corrosion Science*, 1997, **39**, 969-980.
32. G. Henkelman, A. Arnaldsson and H. Jónsson, *The Journal of Chemical Physics*, 2006, **124**, 2161193.
33. A. Michaelides, P. Hu and A. Alavi, *The Journal of Chemical Physics*, 1999, **111**, 1343-1345.
34. V. Ledentu, W. Dong and P. Sautet, *J Am Chem Soc*, 2000, **122**, 1796-1801.
35. J. Greeley and M. Mavrikakis, *Surface Science*, 2003, **540**, 215-229.
36. V. R. Galakhov, E. Z. Kurmaev, K. Kuepper, M. Neumann, J. A. McLeod, A. Moewes, I. A. Leonidov and V. L. Kozhevnikov, *The Journal of Physical Chemistry C*, 2010, **114**, 5154-5159.
37. Y. Ebisuzaki, W. J. Kass and M. O'Keeffe, *The Journal of Chemical Physics*, 1967, **46**, 1378-1381.
38. X. Lu, T. Depover and R. Johnsen, *Int J Hydrogen Energ*, 2022, **47**, 31673-31683.
39. S. P. Zholobov and M. D. Malev, *Soviet Physics Technical Physics*, 1971, **16**, 488.
40. J.-W. Park and C. J. Altstetter, *Metallurgical Transactions A*, 1987, **18**, 43-50.
41. C. Mitra, T. Meyer, H. N. Lee and F. A. Reboredo, *The Journal of Chemical Physics*, 2014, **141**.
42. M. David, A. Prillieux, D. Monceau and D. Connétable, *Journal of Alloys and Compounds*, 2020, **822**, 153555.
43. H. Z. Fang, S. L. Shang, Y. Wang, Z. K. Liu, D. Alfonso, D. E. Alman, Y. K. Shin, C. Y. Zou, A. C. T. van Duin, Y. K. Lei and G. F. Wang, *J Appl Phys*, 2014, **115**, 043501.

The main generated data for this study was already included in the manuscript. As for the raw/processed data required to reproduce these findings, through communications, we can share them to the readers if they need. The software we used for this study is VASP 5.4.3. Here we revised the Data availability as following:

"The raw/processed data required to reproduce these findings cannot be shared at this time due to technical or time limitations but may be obtained by contacting corresponding author. The VASP software can be found at www.vasp.at. The version of VASP employed for this study is 5.4.4.